ACS OMEGA

http://pubs.acs.org/journal/acsodf

Article

Direct CO_2 Capture from Air via Crystallization with a Trichelating Iminoguanidine Ligand

He Cai, Xingwang Zhang, Lecheng Lei, and Chengliang Xiao*

Cite This: *ACS Omega* 2020, 5, 20428−20437

Read Online

ACCESS | Metrics & More | Article Recommendations | Supporting Information

ABSTRACT: Effectively reducing the concentration of CO_2 in ambient air is essential to mitigate global warming. Existing carbon capture and storage technology can only slow down the carbon emissions of large point sources but cannot treat the already accumulated CO_2 in the environment. Herein, we demonstrated a simple direct CO_2 capture method from air via reactive crystallization with a new trichelating iminoguanidine ligand (BTIG). It could strongly bind CO_2 to form insoluble carbonate crystals that could be easily isolated. In the crystal, CO_2 was transformed to CO_3^{2-} and trapped in a dense hydrogen bonding network in terms of carbonate−water clusters. This capture process was reversible, and the BTIG ligand could be regenerated by heating the BTIG−CO_2 crystal at a mild temperature, which was much lower than the decomposition temperature of $CaCO_3$ (~900 °C). Thermodynamic and kinetics analyses indicate that the crystallization process was exothermic with an enthalpy of −292 kJ/mol, and the decomposition energy consumption was 169 kJ per mol CO_2. In addition, BTIG could also be employed for CO_2 capture from flue gas with a capacity of 1.46 mol/mol, which was superior to that of most of the reported sorbents.

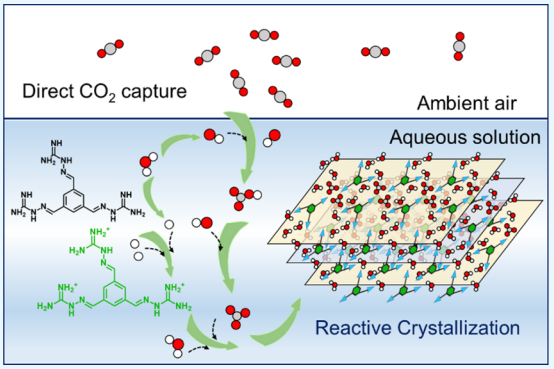

INTRODUCTION

After industrial revolution, anthropogenic carbon emissions and their redistribution in the environment seriously affect Earth's carbon cycle. Since 1980, the atmospheric CO_2 concentration has increased from 340 ppm to more than 413.67 ppm.[1] In total, 645 billion tons of carbon (GtC) has been emitted from 1850 to 2018,[2] leading to a grim environment situation, such as greenhouse effect. Efforts for a significant emission reduction from continuous demand of carbon-source fuel may face risks of economy and politics; therefore, technologies of carbon capture and storage (CCS) for negative CO_2 emission are urgently required.[3−6]

The conventional CCS technologies are mostly used to capture CO_2 in flue gas discharged from large high-concentration point sources like power plant with sorbents or solutions.[7,8] However, about half of the CO_2 emission comes from the dispersed sources such as cars and airplanes that is difficult to collect and is emitted to the atmosphere. In 1999, Lackner et al. proposed a technical idea of extracting CO_2 directly from air,[9] that is direct air capture (DAC) with physical or chemical sorbents. Compared with conventional CCS, this technology can treat the CO_2 emitted from point sources and distributed sources.

Different from flue gas having a CO_2 volume fraction of 5−15%,[10] ambient air is an ultradilute gas system composed of only 0.041% CO_2. To achieve high capture efficiency for DAC, the materials should exhibit strong affinity, high selectivity, and fast kinetics for CO_2. Porous materials such as carbon materials,[11,12] zeolites,[13,14] and metal−organic frameworks[15] have been largely reported for CO_2 sorption, but they were not so efficient due to the weak physical interaction between such sorbents and CO_2, which resulted in a lower capacity and poorer selectivity over N_2 and H_2O molecules under a low CO_2 partial pressure.[16,17] Therefore, the chemisorption materials are more promising for DAC. The simplest materials were aqueous/solid alkaline hydroxides, oxides, and salts such as NaOH, KOH, $Ca(OH)_2$, CaO, and K_2CO_3, which had high binding energy and showed strong affinity for CO_2.[18−22] However, a high calcination temperature of ~900 °C for $CaCO_3$ and ~1000 °C for Na_2CO_3 cost huge energy for regeneration of these sorbents to release CO_2. Amine-based materials have been widely investigated for capturing CO_2 from ambient air. Aqueous solution of amine such as monoethanolamine (MEA) was used in scrubbing industrial flue gas,[23] but toxicity and difficulty of storage limited its large-scale deployment. In addition, due to water evaporation during regeneration, there would be considerable loss of energy. Amine-modified sorbents may overcome the above drawbacks

Received: May 26, 2020
Accepted: July 23, 2020
Published: August 6, 2020

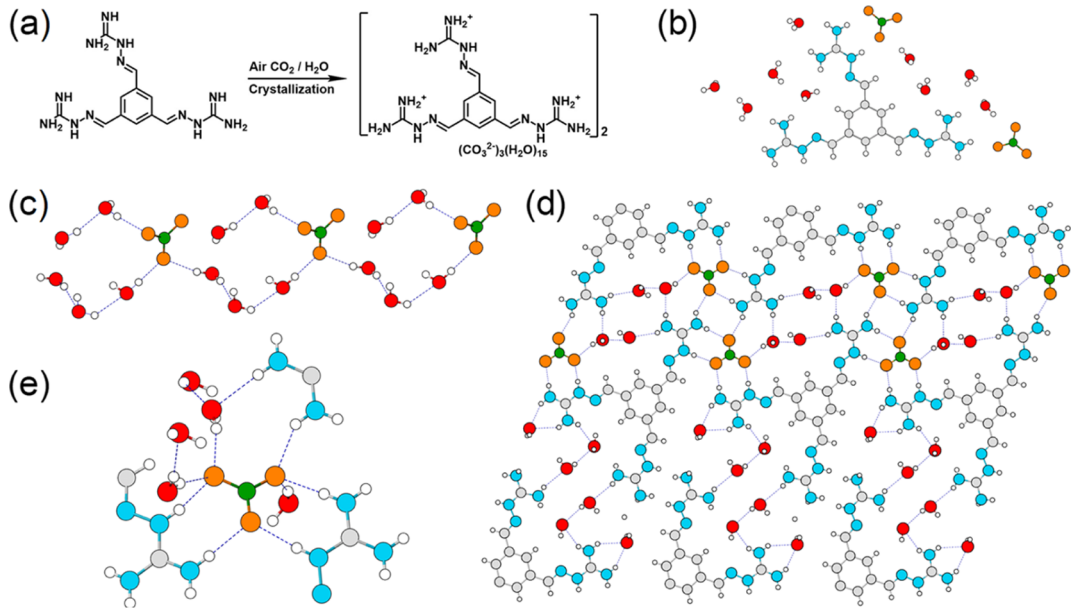

Figure 1. (a) Reaction between BTIG and CO_2, (b) structure of single BTIG molecule surrounded with water and CO_3^{2-}, (c) structure of $[CO_3(H_2O)_5]_n^{2-}$ anion clusters, (d) hydrogen bonding network in BTIG−CO_2 crystal, and (e) one CO_3^{2-} anion trapped in the hydrogen bonding network constructed by water and BTIG molecules (C in $BTIGH_3^{3+}$: gray, N: blue, C in CO_3^{2-}: green, O in CO_3^{2-}: orange, O in H_2O: red, and H: white).

and have gained more attention.[24] Monomers or polymeric amines were loaded into the porous supports such as silica or other novel materials by physical impregnation, chemical graft, or in situ polymerization[25−29] to obtain efficient CO_2 sorbents. However, easy leaching and volatilization of low molecular amines caused by weak physical interaction, lower CO_2 capture capacity caused by less amine content in covalent tethering, and slower kinetics of CO_2 diffusion in the "crowded" polyamine matrix are the issues that need to be addressed.[24] In addition, a new technology idea using humidity swing which avoid the direct heat request has been reported for the DAC process,[30,31] but it still needs further research. Until now, it is still desirable to develop effective materials and methods to properly handle CO_2 in the framework of DAC.

Recently, a type of novel sorbents entitled as phase change sorbents has been widely investigated to capture CO_2. When CO_2 is fixed, the homogeneous sorbent would be divided into CO_2-rich and lean phases which are easy to separate. According to different phase separation mechanisms, biphasic sorbents can be divided into two categories: CO_2-triggered and thermomorphic ones.[32] For type 1 sorbents, such as triethylenetetramine (TETA)/2-(diethylamino)ethanol (DEEA), TETA/*N*,*N*-dimethyl-cyclohexylamine (DMCA), 1,4-butanediamine (BDA)/DEEA, and *N*-methyl-1,3-propane-diamine/DEEA,[33−35] the reaction between them and CO_2 would change the solvent properties such as polarity or ionic strength, resulting in a phase transition. However, the CO_2 capture properties and phase transition were greatly influenced by the composition of biphasic solvents.[32,36−38] Adding a phase splitter such as sulfolane could effectively improve their performance.[39,40] Nonaqueous biphasic solvents such as ionic liquids[41−45] and various alcohols[46−49] are also used for lower heat consumption than water evaporation. For type 2 sorbents, lipophilic amines were partially miscible with water, forming homogeneous or heterogeneous phase,[50] which would change to be homogeneous after CO_2 loading. When heated at a relative low temperature (lower than 100 °C), the CO_2-loaded amines would decompose, resulting in phase separation and amines regeneration simultaneously.[51] Such typical systems are exemplified by *N*,*N*-dipropylamine/DMCA and *N*-methylcyclohexylamine/DMCA.[51,52] Surely, many traditional inorganic material-led CO_2 mineralization processes such as aqueous alkaline solutions or silicates are also being investigated for practical applications.[53]

The phase change sorbents are mostly used in CO_2 capture from flue gas, but they are rarely reported in the DAC process. Iminoguanidine analogues are a type of positively charged organic molecules which can form salts with most oxoanions as anion receptors,[54−56] they were reported first in 1898.[57] Very recently, bis-iminoguanidine molecules such as 2,6-pyridine bis(iminoguanidine) (PyBIG)[58] and glyoxal-bis-(iminoguanidine)[59] were employed as excellent DAC sorbents which hold high capacity and lower regeneration temperature. CO_2 can be captured to the aqueous solution in the natural environment and forms insoluble carbonate salts, the product can be separated by a simple filter. We reasoned that a bigger quasi-plane would be conducive to the formation and stacking of planar hydrogen bonding networks between amino-guanidinium and anionic CO_3^{2-}, which was beneficial for the formed salts to crystallize from the solution phase. Additional more positive charges on each ligand would increase the binding kinetics and CO_2 capacity. Thus, a trichelating iminoguanidine ligand (BTIG) was designed and newly synthesized in this work. The benzene ring in the molecular center provides a rigid planar structure, and three quasi-plane guanidine cation sites contact and capture carbonate ions through electrostatic and hydrogen bonding. The CO_2 capture properties of BTIG were investigated, and the underlying mechanisms were unraveled using a combined structural and thermodynamic method. This work clearly discloses that the trichelating BTIG ligand is a promising material for DAC.

https://dx.doi.org/10.1021/acsomega.0c02460
ACS Omega 2020, 5, 20428−20437

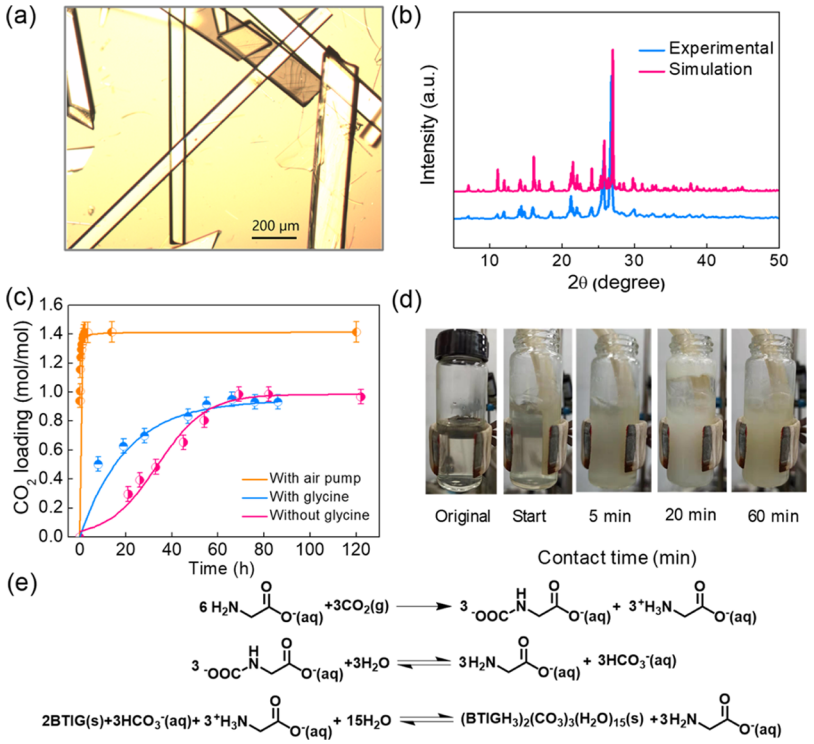

Figure 2. (a) Optical image of BTIG−CO_2 crystals, (b) comparison between experimental PXRD pattern of the bulk crystalline product and the simulated PXRD pattern from the single XRD data, (c) capture kinetics of CO_2 from air by BTIG solution with glycine and without glycine and with an air pump, (d) CO_2 capture from the simulated flue gas by BTIG solution, and (e) capture mechanism of CO_2 by BTIG solution with glycine.

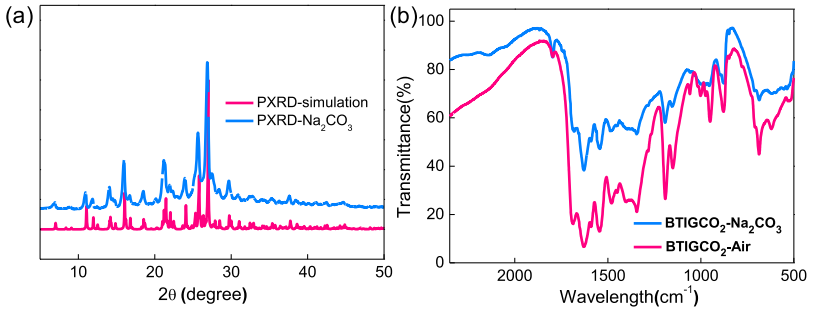

Figure 3. (a) Comparison between experimental PXRD patterns of the BTIG−CO_2 product obtained by adding Na_2CO_3 to BTIG·3HCl and the simulated PXRD pattern from the single-crystal X-ray data and (b) comparison between FT-IR spectra of BTIG−CO_2 obtained by air capture and adding Na_2CO_3.

RESULTS AND DISCUSSION

Synthesis and Structure. Imine condensation of 1,3,5-benzene-tricarboxaldehyde and aminoguanidinium chloride in ethanol, followed by neutralization with aqueous NaOH yielded the 1,3,5-benzene-tri(iminoguanidine) (BTIG, Figure 1a) ligand. This reaction is fairly mild, and the final product can be facilely prepared on a large scale.

CO_2 can be easily captured by the BTIG ligand even from the atmosphere (Figure 1a). When letting an aqueous solution of BTIG open to the ambient air for two days, some faint yellow single crystals of BTIG−CO_2 with a size of several hundred micrometers (Figure 2a) were obtained. The structure of BTIG−CO_2 was solved well by the single-crystal X-ray diffraction (XRD) technique, and the theoretical formula of BTIG−CO_2 was determined to be $(BTIGH_3)_2(CO_3)_3(H_2O)_{15}$ based on the charge balance and the repeating unit in anionic clusters. The structure contains cationic $BTIGH_3^{3+}$, CO_3^{2-} anions, and H_2O molecules (Figure 1b). Gaseous CO_2 molecules are strongly trapped in a dense hydrogen bonding network in terms of CO_3^{2-} anions. Carbonate anions are linked by nearby water molecules to form "chain-like" anionic clusters, $[CO_3(H_2O)_5]_n^{2-}$, where each CO_3^{2-} accepts three water hydrogen bonds of O−H···O with a distance range of 1.897−1.976 Å (Figure 1c). In addition, three $BTIGH_3^{3+}$ cations in the same plane are involved to bind one CO_3^{2-} via electrostatic interactions and multiple hydrogen bonds between H atoms of guanidine and the carbonate ion, thereby extending into a huge quasi-planar hydrogen bonding network (Figure 1d). Each CO_3^{2-} anion accepts five N−H···O bonds within a distance range of 1.870−2.057 Å (Figure 1e). Networks are stacked in a dislocation parallel manner, and the anion clusters shuttle through gaps between the cations obliquely, reinforcing the stacking effect (Figure S4). Comparing the Fourier transform infrared (FT-

https://dx.doi.org/10.1021/acsomega.0c02460
ACS Omega 2020, 5, 20428−20437

IR) spectrum of BTIG−CO_2 crystal with the original BTIG ligand, strong broad peaks at 1344 and 1400 cm^{-1} were newly found, corresponding to the incorporated carbonate ion (Figure 4b). The purity of the crystal phase was confirmed by powder XRD (PXRD) analysis, which matched well with the data from the single XRD measurement (Figure 2b).

CO_2 Capture from Air and Flue Gas. Though CO_2 can be captured directly by BTIG in the solution to form large pure crystals under low partial pressure, this gas−liquid−solid process has a slow reaction kinetics and always needs several days to reach the equilibrium. In the crystallization separation process, CO_2 is bound in the form of carbonate ions, so there should be a conversion step from CO_2 in the gas phase to CO_3^{2-} in the liquid phase. Meanwhile, free BTIG ligands in the solution transform into $BTIGH_3^{3+}$ cations through a protonation process. These two conversions are relatively slow in a passive condition such as DAC. As a comparative experiment, a 5−6 equiv concentration of sodium carbonate solution was added dropwise to BTIG·3HCl and BTIG solution (8.66 mM, 5 mL); a precipitate was formed immediately in the former and no reaction was found in the latter (Figure 3a,b). On the contrary, a precipitate occurred when a sodium bicarbonate solution was added to the BTIG solution because bicarbonate anions could provide protons to BTIG.[58] The result indicates that the protonated $BTIGH_3^{3+}$ could react with carbonate anions, and this process was relatively fast. Therefore, it is the ionization of CO_2 and the protonation of BTIG that limit the rate of the entire reaction. Considering that the BTIG·3HCl salt shows no capability of binding CO_2 directly from air, free BTIG ligand is a better choice. Thus, raising the rate of CO_2 diffusion to the solution and transformation into anions seem to be an efficient way to obtain a faster kinetics. Many conventional sorbents such as alkali solution and amine can help to accelerate this process. As a nontoxic and environment friendly material, glycine has been reported to have a strong capability of converting CO_2 into anions in the solution through a zwitterionic mechanism.[58,60] In our experiments, aqueous solution of BTIG (6 mM, 5 mL) and aqueous solution of BTIG/glycine (6 mM/10 mM, 5 mL) were comparatively employed for direct CO_2 capture from air. The results of reaction kinetics are shown in Figure 2c. For both systems, CO_2 could be efficiently captured from air, and the obtained weight of solid BTIG−CO_2 crystals increased as a function of standing time. Obviously, the crystallization process of BTIG−CO_2 with glycine was about twice faster than that without glycine. For example, the weight of BTIG−CO_2 was measured to be 7.0 mg at a standing time of 19 h with glycine in the solution while it was only 3.3 at 21 h without added glycine. The overall crystallization process is briefly summarized in Figure 2e. The CO_2 loading of neat BTIG solution was about 0.99 mol/mol, as shown in Figure 2c. This value is slightly lower in BTIG/glycine solution because that CO_2 is fixed by glycine in the form of carbamate and the figure only covers the carbonate anions in the crystal. In addition, the CO_2 capture performance from air could be greatly enhanced by artificially applying a driving force. In a simple air bubbling process with the most common and economical air pump, the BTIG aqueous solution of the same concentration (6 mM, 50 mL) showed much more rapid kinetics with only 2 h and higher CO_2 loading with 1.4 mol/mol, respectively (Figures 2c and S5d).

In practical utilization, BTIG can also be used for flue gas capture besides DAC. A simulated flue gas composed of CO_2/N_2 (13/87%) at a flow rate of 0.2 L/min was bubbled into an aqueous solution of BTIG (10 mM, 10 mL). A precipitate formed immediately at the beginning, and for complete precipitation, the bubble time was extended to 1 h (Figure 2d). UV−vis spectrum analysis of the residual liquid shows that 97% of BTIG ligands have reacted with CO_2 and crystallized from the liquid phase, corresponding to a capacity of about 1.46 mol CO_2 per mol of BTIG (Figure S6). This value represents a very high capture capacity of CO_2, which is higher than those of MEA solution[39,61] and biphasic solvents systems[33] which are shown in Table 1. Even in the DAC process without any artificial driving force, the CO_2 capacity of BTIG (0.99 mol/mol) still exceeds that of these materials. Using similar guanidinium ligands for comparison, the total CO_2 capacity (carbonate and carbamate) of PyBIG with assistance of potassium glycinate in the DAC process is about 0.7 mol/mol;[58] this value of GBIG was not reported in the reference. Correspondingly, the CO_2 loading of GBIG in flue gas capture is about 1.78 mol/mol.[59] It can be found that CO_2 capacity of BTIG is much higher than PyBIG in DAC but lower than GBIG in flue gas capture. This proves that increasing the charge number of the ligand molecule actually improves the capacity. Different from BTIG and PyBIG, what GBIG−CO_2 contains is not carbonate but bicarbonate anion, that is the reason why this two-charged ligand has an unusual high CO_2 capacity. The reason for this change in the capture mechanism needs further research. The CO_2 concentration and flow velocity of the airflow in this flue gas test are much higher than natural air, which makes the capture performance of BTIG much better than that in the case of DAC, and the sorption kinetics is also improved to tens of times of the DAC process.

Table 1. Comparison of CO_2 Loading between BTIG and Common Sorbents

sorbents	concentration of the sorbents	operating condition	CO_2 loading (mol/mol)	reference
BTIG solution	0.01 M	[a]	1.46	this study
pure MEA aqueous solution	30 wt %	[b]	0.67	60
MEA/sulfolane solution	4/5 M	[c]	1.00	39
BDA/DMCA	5 mol/kg, a concentration level similar to 30 wt % MEA, the molar ratio of two components is 3:7	[d]	0.70	33
BDA/DEEA			0.87	
DETA/DMCA			0.65	
DETA/DEEA			0.88	
TETA/DMCA			0.65	
TETA/DEEA			0.91	

[a]CO_2 concentration (volume fraction): 13%, gas flow rate: 200 mL/min, pressure: atmosphere. [b]CO_2 concentration (volume fraction): 15%, gas flow rate: 100.2 mL/min, pressure: atmosphere. [c]CO_2 concentration (volume fraction): 15%, gas flow rate: 1800 mL/min, pressure: atmosphere. [d]CO_2 concentration: pure CO_2, gas flow rate: 105, pressure: atmosphere.

Regeneration by Heating. Efficient regeneration of the ligand is the key to the operation of sorption and desorption cycles. Most of the sorbents are regenerated by heating, which will waste large amounts of energy. Inorganic sorbents such as

https://dx.doi.org/10.1021/acsomega.0c02460
ACS Omega 2020, 5, 20428−20437

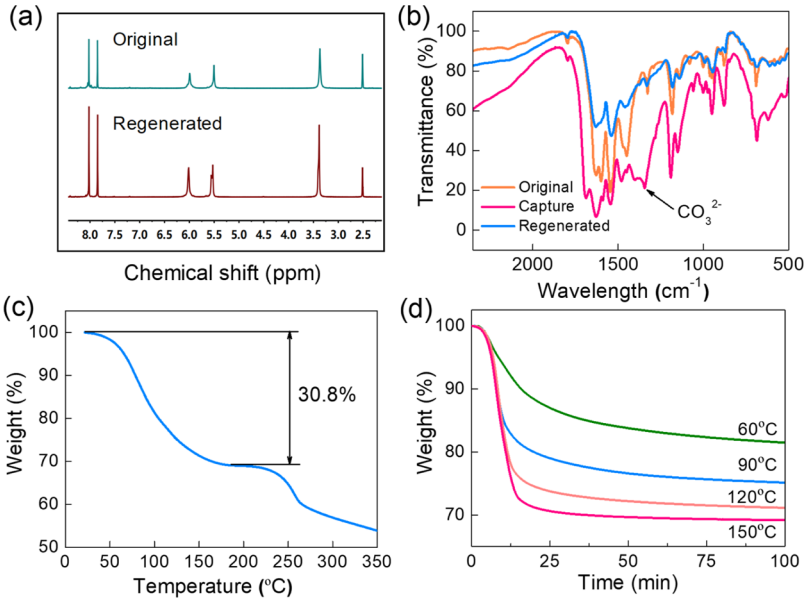

Figure 4. Regeneration of BTIG. (a) ^{1}H NMR patterns of original and regenerated BTIG ligand, (b) FT-IR spectra of original BTIG, BTIG−CO_2, and regenerated BTIG, (c) temperature-ramped TGA curve, and (d) isothermal TGA curves at 60, 90, 120, and 150 °C.

CaO and NaOH need high temperature to regenerate, while aqueous amine sorbents will consume huge energy on the water evaporation for releasing CO_2. In our case, after sorption, the resulting BTIG−CO_2 solids can be easily isolated from solution and regenerated by heating at a relatively low temperature.

Thermogravimetric analysis (TGA) was used to characterize the decomposition of BTIG−CO_2 crystals. In a temperature-ramped TGA measurement, 30.8% mass reduction was observed in the range of 50−150 °C (Figure 4c). This reduction was attributed to the decomposition of BTIG−CO_2 to BTIG ligand. From the ^{1}H-NMR spectrum of the regenerated ligand (Figure 4a) which is the same as the free ligand and without other water peaks except for the solvent one, it can be considered that BTIG−CO_2 decomposed completely and changed into BTIG. However, the mass reduction rate in TGA is inconsistent with the expected weight loss of 40% for $(BTIGH_3)_2(CO_3)_3(H_2O)_{15}$. This may be caused by weathering dehydration during crystal storage, the actual stoichiometric should be $(BTIGH_3)_2(CO_3)_3(H_2O)_{6.5}$ with a theoretical weight loss of 30.8%. In isothermal TGA measurements at 60, 90, 120, and 150 °C, the weight of the samples decreased and remained at a certain value for a period of time (Figure 4d). Especially, the crystals showed complete decomposition at 150 °C after 25 min with no additional weight loss even after 75 min, which indicates that the BTIG ligand has an excellent thermal stability at the regeneration temperature. The BTIG−CO_2 samples for ^{1}H NMR and FT-IR analyses were heated in a vacuum oven at 150 °C for 10 h. After heating, the peak of CO_3^{2-} in the FT-IR spectra (Figure 4b) disappeared, and the ^{1}H NMR spectra were exactly the same as the original ligand, which indicates that BTIG−CO_2 could be converted to BTIG at this temperature.

We then performed rough kinetic analysis on the thermogravimetric data under constant temperature. After subtracting the preparation time t_0 of the heating section, the values of the pyrolysis fraction conversion rate α and the time $t-t_0$ at different temperatures could be obtained (Figure S7a). By fitting the kinetic models of several common solid reactions [Avrami−Erofeev, Prout−Tompkins, and geometrical phase boundary (Figure S8−S10)],[59] it is found that the decomposition of BTIG−CO_2 accords best with the Avrami−Erofeev model (eq 1, Figure S7b), corresponding to the random nucleation and then the growth mechanism.

$$-\ln(1-\alpha) = kt \quad (1)$$

The rate constant k of the decomposition at each temperature could be obtained from the slope of the fitted curve, on a basis of which the Arrhenius plot of this reaction could be made (Figure S7c). The activation barrier E was calculated to be 17.9 kJ/mol, which was a relatively low value.

Thermodynamic Analysis of the Entire Cycle. Analysis of the mechanism of sorption and regeneration and measurements of their thermodynamic parameters are vital to understand the energy consumption in the entire cycle. The process of BTIG capturing CO_2 is similar to PyBIG.[58] As depicted in Figure 5, in the process of capturing CO_2 from air, BTIG dissolves in water and takes protons from water molecules to generate $BTIGH_3^{3+}$ cations and OH^- (eqs 2 and 3). CO_2 diffuses into the solution and forms HCO_3^- with OH^-. The HCO_3^- anion further reacts with OH^- to yield CO_3^{2-} (eqs 4−6). The CO_3^{2-} anion reacts with the $BTIGH_3^{3+}$ cation and is removed from the solution by crystallization (eq 7). The overall reaction is shown in eq 8. These reaction steps can explain why BTIG·3HCl cannot be used in the DAC process mentioned earlier. It is OH^- that reacts directly with CO_2, and the protonated ligand in the solution cannot produce OH^-. The enthalpy of eq 2 was determined to be 49 kJ/mol by variable-temperature solubility measurements and van't Hoff plot fitting of BTIG (Figure S11). This positive value shows that the protonation of BTIG is an endothermic process, which is consistent with those of similar ligands reported in the literatures.[59] Enthalpy values of eqs 4−6 are −58.2, −150, and −121 kJ/mol, respectively.[62−65] The formation ΔH of CO_3^{2-} was calculated by adding the enthalpies of HCO_3^- dissociation and the reaction of H^+ and OH^- to generate water. The ionization from CO_2 in the gas phase to CO_3^{2-} in the solution is an exothermic process with a ΔH of −329.2 kJ/mol. The

https://dx.doi.org/10.1021/acsomega.0c02460
ACS Omega 2020, 5, 20428−20437

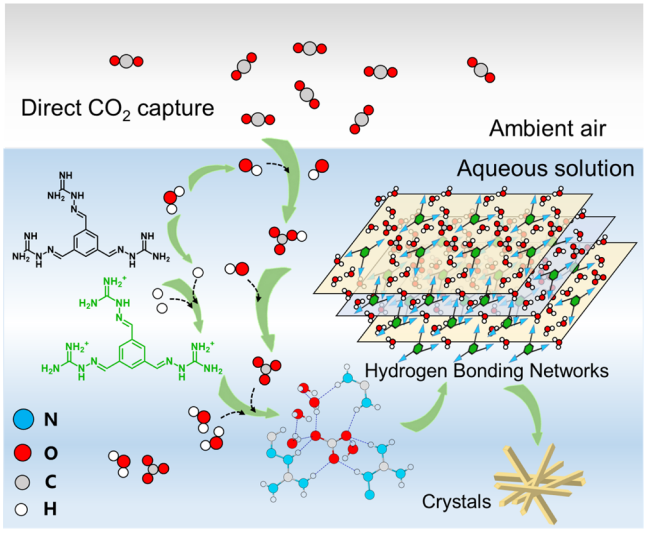

Figure 5. Mechanism schematic of CO_2 capture from air into BTIG aqueous solution. The yellow and blue alternating sheets mean that the molecules belong to different planes.

ΔH of the crystallization step (eq 7) was calculated to be −292 kJ/mol using a similar method in eq 2 (Figure 6a,b), which is an exothermic process. Therefore, by adding the enthalpy of eqs 4−7, the process of CO_2 being captured by BTIG aqueous solution from air through crystallization is energetically favorable with a ΔH of −207.1 kJ per mol CO_2. It should be noted that this value represents the process of CO_2 fixation from the gas phase to crystal (eqs 3−7) and is not the enthalpy of the overall reaction (eq 8).

$$2\mathrm{BTIG(s)} \rightleftharpoons 2\mathrm{BTIG(aq)} \quad (2)$$

$$2\mathrm{BTIG(aq)} + 6\mathrm{H_2O} \rightleftharpoons 2\mathrm{BTIGH_3^{3+}(aq)} + 6\mathrm{OH^-} \quad (3)$$

$$3\mathrm{CO_2(g)} \rightleftharpoons 3\mathrm{CO_2(aq)} \quad (4)$$

$$3\mathrm{CO_2(aq)} + 3\mathrm{OH^-} \rightleftharpoons 3\mathrm{HCO_3^-(aq)} \quad (5)$$

$$3\mathrm{HCO_3^-(aq)} + 3\mathrm{OH^-} \rightleftharpoons 3\mathrm{CO_3^{2-}(aq)} + 3\mathrm{H_2O} \quad (6)$$

$$2\mathrm{BTIGH_3^{3+}(aq)} + 3\mathrm{CO_3^{2-}(aq)} + 15\mathrm{H_2O} \rightleftharpoons (\mathrm{BTIGH_3})_2(\mathrm{CO_3})_3(\mathrm{H_2O})_{15}\mathrm{(s)} \quad (7)$$

$$2\mathrm{BTIG(s)} + 3\mathrm{CO_2(g)} + 15\mathrm{H_2O} \rightleftharpoons (\mathrm{BTIGH_3})_2(\mathrm{CO_3})_3(\mathrm{H_2O})_{15}\mathrm{(s)} \quad (8)$$

Ligand regeneration is critical for its practical application, so differential thermal analysis (DTA) and differential scanning calorimetry (DSC) were used to analyze the decomposition of BTIG−CO_2. The DTA curve (Figure 6c) shows an obvious endothermic peak in the range of 60−150 °C which coincides with the result of TGA. During this process, the BTIG−CO_2 crystals absorbed heat to make it decompose and release CO_2 and water. The DSC measurement was performed in the range of 0−200 °C (Figure 6d), and the decomposition heat of 507.3 kJ/mol was obtained by the integrated area. The enthalpy of 1 mol CO_2 release was calculated to be 169 kJ/mol. This value includes the energy need of CO_2 and H_2O separation. Because the crystal lose a few water molecules as mentioned before, the actual formula is $(\mathrm{BTIGH_3})_2(\mathrm{CO_3})_3(\mathrm{H_2O})_{6.5}$, so the ratio of H_2O and CO_2 release is approximately 6.5:3. The energy consumption of water molecules released from BTIG−CO_2 can be estimated by the heat of water vaporization (40.63 kJ/mol). Thus, the energy consumption for CO_2 molecule separation alone is about 81 kJ per mol CO_2, which is much lower than that of $CaCO_3$ decomposition[66] (177.8 kJ/mol). Different from the "$CaCO_3$ process," much energy was not used for CO_2 release but for water evaporation which increases the cost of ligand regeneration. In practical applications, the calories in high-temperature vapor could be recovered by heat exchanger which is very mature in the industry, so this limitation can be overcome with the assistance of existing technology. The overall energy consumption is theoretically lower than the conventional "$CaCO_3$ process." The energy consumption of PyBIG is 223 kJ/mol (including water evaporation) or 75 kJ/mol (CO_2 separation alone), and this

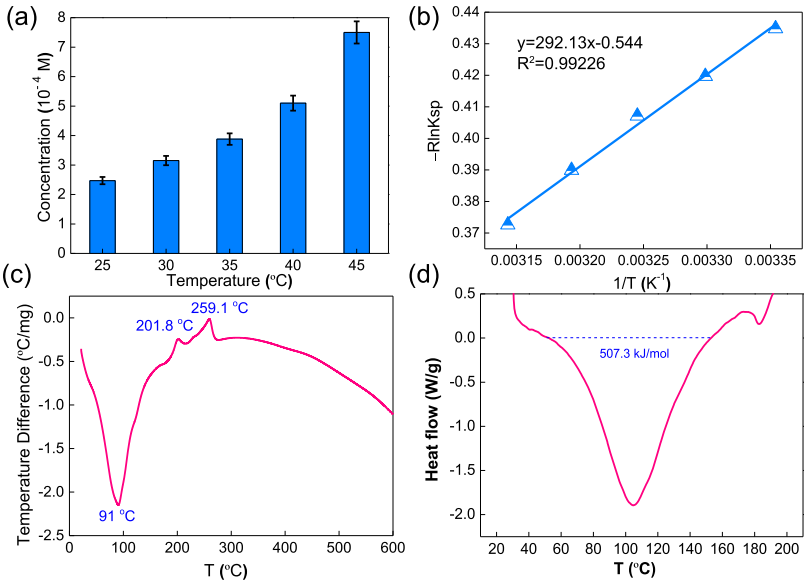

Figure 6. Thermodynamic analysis of CO_2 capture and release. (a) Concentration of saturated solution of BTIG−CO_2 at different temperatures, (b) van't Hoff plot fitting of the crystallization step (eq 7), and (c) DTA and (d) DSC analysis curves of BTIG−CO_2 decomposition.

https://dx.doi.org/10.1021/acsomega.0c02460
ACS Omega 2020, 5, 20428−20437

value of GBIG is 121.5 kJ/mol and 40 kJ/mol, respectively. BTIG's regeneration energy consumption is comparable to PyBIG, which is even lower when considering the energy consumed by water molecules, but it is higher than GBIG's. As mentioned before, GBIG has different sorption and decomposition mechanisms as reported,[59] the process of bicarbonate detachment from the crystal and conversion to CO_2 is different from BTIG and PyBIG, which may be the reason for its unusual low-energy consumption.

CONCLUSIONS

In this work, a trichelating iminoguanidine ligand (BTIG) was designed and newly synthesized for direct CO_2 capture from air. Under an ultradilute condition, BTIG aqueous solution could efficiently extract CO_2 from ambient air through reactive crystallization. It is found that CO_2 was tapped in the crystals in the form of CO_3^{2-} that strongly attached to the cationic BTIG and water via electrostatic interactions and hydrogen bonds. The ligand could be easily regenerated by heating under a relatively mild condition of 60−150 °C. Through thermodynamic analysis of the sorption and regeneration process, the capture of CO_2 was an energy favorable exothermic step, and the regeneration of BTIG ligand needed a heat consumption of 81 kJ per mol CO_2. In addition, BTIG could also be employed for CO_2 capture from flue gas with a capacity of 1.46 mol/mol, which was superior to that of most of the reported sorbents. Compared with similar guanidine-based ligands, the CO_2 capacity has increased, and BTIG has considerable energy consumption for regeneration. Consequently, in the framework of DAC technology, we provide a facile and efficient method to directly sequester CO_2 from air on the basis of reactive crystallization with a newly designed trichelating iminoguanidine ligand.

EXPERIMENTAL SECTION

Materials and Methods. All reagents were purchased and used without further purification. 1,3,5-Benzenetricarboxaldehyde (>98 wt %) was purchased from Jilin Chinese Academy of Science-Yanshen Technology Co., Ltd. Aminoguanidinium chloride (>99 wt %) was purchased from Shanghai Macklin Biochemical Co., Ltd, China. PXRD measurements were carried out with a Rigaku Ultima IV diffractometer using Cu Kα radiation (λ = 1.54184 Å). Single-crystal X-ray data were collected on a Bruker D8-Venture diffractometer with a Turbo X-ray Source (Mo Kα radiation, λ = 0.71073 Å). Nuclear magnetic resonance spectra were collected on a Bruker AVANCE III 500. FT-IR spectra were collected using a Thermo iS50 FT-IR spectrometer. TGA and DTA were conducted with a SDT Q600 V20.9 Build 20 instrument. DSC measurements were conducted with a METTLER-TOLEDO DSC 1/400 instrument.

Synthesis and Characterization of BTIG. 1,3,5-Benzenetricarboxaldehyde (0.4237 g, 2.5 mmol) was suspended in 50 mL of absolute ethanol, and then, aminoguanidinium chloride (1.3 g, 10 mmol) was added. The mixture was magnetically stirred and heated to 60 °C for 8 h. As the reaction began, the product was precipitated out of solution as a white solid. After 8 h, 1.08 g of BTIG·3HCl was obtained by vacuum filtration and washed with ethanol (yield: 93%).

BTIG·3HCl (1.00 g, 2.28 mmol) was dissolved in a certain amount of deionized water (~25 mL), and NaOH (0.28 g, 7 mmol, dissolved in 1−2 mL water) was added. The resulting solution became deep maroon immediately and was stirred under room temperature until a faint yellow precipitate appeared (about 48 h). The final product (BTIG) was isolated by filtration, rinsed with cold water, and dried in a vacuum oven under 50 °C for 4 h. Yield: 77% (0.5760 g). ^{1}H NMR (500 MHz, DMSO-d_6): δ (ppm) = 8.02 (3H, s), 7.85 (3H, s), 6.01 (6H, bs), 5.53 (6H, bs). ^{13}C NMR (125 MHz, DMSO-d_6): δ (ppm) = 161.09, 143.67, 137.61, 124.00.

Synthesis of BTIG−CO_2 and Single-Crystal Structure. Aqueous solution of BTIG (8.66 mM, 5 mL for each bottle) was placed in several 20 mL strain bottles and put in air. After 12 h, the solution became cloudy, and some small crystals were formed on the bottom. Two days later, long acicular crystals were found in the solution with a color of faint yellow under a stereomicroscope.

Direct CO_2 Capture from Air. Aqueous solution of BTIG (6 mM, 5 mL for each bottle) was placed in eight 20 mL strain bottles and left open to the ambient air. After a certain time (21, 26, 33, 45, 54, 69, 82, and 122 h), the solution of one bottle was filtered, rinsed with water, allowed to dry, and weighted. For comparison, 10 mM of glycine was added into each bottles containing 6 mM of BTIG. The operation was similar to the above except of the sampling time (8, 19, 28, 47, 55, 66, 76, and 86 h).

TGA/DTA/DSC Measurements and BTIG Regeneration. *TGA.* The sample (BTIG−CO_2, 11.2970 mg) was placed under a nitrogen atmosphere at a flow rate of 100 mL/min and then ramped at 5 °C/min to 615 °C. DTA was operated under the same condition. DSC measurement was conducted under a nitrogen atmosphere at a 10 °C/min heating rate to 200 °C. For the isothermal TGA, samples were placed under a nitrogen atmosphere at a flow rate of 120 mL/min, then ramped at 10 °C/min to the corresponding temperature (60, 90, 120, 150 °C, respectively) and maintained until the weight did not change.

BTIG Regeneration. The sample was placed on the bottom of a strain bottle and heated in the vacuum oven at 150 °C for 10 h.

Variable-Temperature Solubility Measurements. The solubility of BTIG and BTIG−CO_2 in water was determined by UV−vis spectroscopy. The solubility standard curve was obtained by measuring the absorbance of a series of BTIG and BTIG·3HCl standard solution (1×10^{-5}, 8×10^{-6}, 5×10^{-6}, 2.5×10^{-6}, 1×10^{-6}, and 5×10^{-7} M). The curves are shown in Figure S2. Excess amounts of BTIG and BTIG−CO_2 solid were suspended in 10 mL of deionized water in 15 mL centrifuge tubes separately. The mixture was placed in a thermostatic water bath with a heating apparatus set at 25, 30, 35, 40, or 45 °C for 24 h (Figure S3 confirms that the equilibrium has been reached in 24 h). Subsequently, 2 mL of samples were filtered through a 0.22 μm syringe filter and diluted to the appropriate multiple (100 times for BTIG−CO_2 and 10,000 times for BTIG) for UV−vis analysis. The pH values of saturated solution were measured with a pH meter. All the measurements were taken three times. The obtained solubility, pH values, and K_{sp} are shown in Table S1. The solubility product of $(BTIGH_3)_2(CO_3)_3(H_2O)_{15}$ was calculated by the following formula.[50] At 25 °C, the pK_a of HCO_3^- is 10.32, and the pH value of the saturated solution of BTIG−CO_2 is 8.33, so the concentration of CO_3^{2-} is 7.51×10^{-6} M according to the definition of pK_a. The concentration of $BTIGH_3^{3+}$ cations was obtained from UV−vis analysis. The

https://dx.doi.org/10.1021/acsomega.0c02460
ACS Omega 2020, 5, 20428−20437

activity coefficients $\gamma\pm$ were estimated by the Debye−Huckel limiting law.

$$K_{sp} = (\gamma \pm)^5[BTIGH_3^{3+}]^2[CO_3^{2-}]^3 = (0.72)^5$$
$$[4.94 \times 10^{-4}]^2[7.51 \times 10^{-6}]^3 = 1.94 \times 10^{-23}$$

CO_2 Capture from Air in a Bubbling Process. Aqueous solution of BTIG (6 mM, 50 mL) was placed in a 100 mL breaker, and then, the air was pumped into it with a porous gas distributor (Figure S5a), meanwhile magnetic stirring was performed to make the whole system evenly dispersed. After about 3 h, CO_2 was saturated in the solution and precipitated as a faint yellow solid (Figure S5b). Taking this moment as the starting point, after a certain time (5 min, 10 min, 15 min, 30 min, 45 min, 60 min, 1.25 h, 1.5 h, 2 h, 2.5 h, 3.5 h, 14 h, and 120 h), 0.5 mL of samples were filtered through a 0.22 μm syringe filter and diluted to 1000 times. The diluted samples were measured by UV−vis spectroscopy to determine the concentration of remaining BTIG and calculate the value of CO_2 loading. The air pump (SOBO model, China) used in this work is the most common product with a gas flow rate of 3.5 L/min (Figure S5c).

CO_2 Capture from Flue Gas. Aqueous solution of BTIG (10 mM, 15 mL) was placed in a 30 mL strain bottle, and then, the flue gas composed of 13% CO_2 and 87% N_2 was bubbled into it for 1 h at a flow rate of 0.2 L/min. A faint yellow precipitate was formed immediately. After 1 h, the solid was separated by a vacuum filter, and the liquid phase was measured by UV−vis spectroscopy to determine the concentration of remaining BTIG.

■ ASSOCIATED CONTENT

Supporting Information

The Supporting Information is available free of charge at https://pubs.acs.org/doi/10.1021/acsomega.0c02460.

1H-NMR and 13C-NMR patterns of BTIG; standard solubility curve of BTIG and BTIG·3HCl; UV spectra of supernatant after shaking excess BTIG; stacks of hydrogen bonding networks in BTIG crystals; experimental device of CO_2 capture from air; UV spectrum of residual liquid from simulated flue gas capture experiment; kinetic analysis of BTIG-CO_2 decomposition; fitting curves of kinetics data to Prout−Tompkins model, geometrical phase boundary model, and Avrami−Erofeev model; van't Hoff plot fitting of BTIG dissolution step; and pH and solubility data of BTIG and BTIG-CO_2 at different temperatures (PDF)

Crystallographic data of BTIG-CO_2 crystal (CIF)

■ AUTHOR INFORMATION

Corresponding Author

Chengliang Xiao − *College of Chemical and Biological Engineering, Zhejiang University, Hangzhou 310027, China;* orcid.org/0000-0001-5081-2398; Email: xiaoc@zju.edu.cn

Authors

He Cai − *College of Chemical and Biological Engineering, Zhejiang University, Hangzhou 310027, China*

Xingwang Zhang − *College of Chemical and Biological Engineering, Zhejiang University, Hangzhou 310027, China;* orcid.org/0000-0002-8564-4678

Lecheng Lei − *College of Chemical and Biological Engineering, Zhejiang University, Hangzhou 310027, China*

Complete contact information is available at: https://pubs.acs.org/10.1021/acsomega.0c02460

Notes

The authors declare no competing financial interest.

■ ACKNOWLEDGMENTS

This work is supported by the National Natural Science Foundation of China (nos. 21876124 and U1732112) and the Fundamental Research Funds for the Central Universities (2020QNA4035).

■ REFERENCES

(1) Trends in Atmospheric Carbon Dioxide; Earth System Research Laboratory, Global Monitoring Division, NOAA. https://www.esrl.noaa.gov/gmd/ccgg/trends/global.html (accessed Nov, 2019.

(2) Friedlingstein, P.; Jones, M. W.; O'Sullivan, M.; Andrew, R. M.; Hauck, J.; Peters, G. P.; Peters, W.; Pongratz, J.; Sitch, S.; Le Quéré, C.; et al. Global carbon budget 2019. *Earth Syst. Sci. Data* **2019**, *11*, 1783−1838.

(3) Jarvis, A. J.; Leedal, D. T.; Hewitt, C. N. Climate−society feedbacks and the avoidance of dangerous climate change. *Nat. Clim. Change* **2012**, *2*, 668−671.

(4) Hansen, J.; Sato, M.; Kharecha, P.; von Schuckmann, K.; Beerling, D. J.; Cao, J.; Marcott, S.; Masson-Delmotte, V.; Prather, M. J.; Rohling, E. J.; et al. Young people's burden: requirement of negative CO_2 emissions. *Earth Syst. Dynam.* **2017**, *8*, 577−616.

(5) Sanz-Pérez, E. S.; Murdock, C. R.; Didas, S. A.; Jones, C. W. Direct capture of CO_2 from ambient air. *Chem. Rev.* **2016**, *116*, 11840−11876.

(6) Bui, M.; Adjiman, C. S.; Bardow, A.; Anthony, E. J.; Boston, A.; Brown, S.; Fennell, P. S.; Fuss, S.; Galindo, A.; Hackett, L. A.; et al. Carbon capture and storage (CCS): the way forward. *Energy Environ. Sci.* **2018**, *11*, 1062−1176.

(7) da Silva, E. F.; Booth, A. M. Emissions from postcombustion CO_2 capture plants. *Environ. Sci. Technol.* **2013**, *47*, 659−660.

(8) D'Alessandro, D. M.; Smit, B.; Long, J. R. Carbon dioxide capture: prospects for new materials. *Angew. Chem., Int. Ed.* **2010**, *49*, 6058−6082.

(9) Lackner, K. S.; Grimes, P.; Ziock, H. J. Capturing carbon dioxide from air. In *Carbon Capture Storage: CO_2 Management Technologies*; Bandyopadhyay, A., Ed.; Apple Academic Press: New York, NY, 2014; pp 363−376.

(10) Jones, C. W. CO_2 capture from dilute gases as a component of modern global carbon management. *Annu. Rev. Chem. Biomol. Eng.* **2011**, *2*, 31−52.

(11) Zhu, X.-L. L.; Wang, P. Y.; Peng, C.; Yang, H.; Yan, X. B. Activated carbon produced from paulownia sawdust for high-performance CO2 sorbents. *Chin. Chem. Lett.* **2014**, *25*, 929−932.

(12) Jiménez, V.; Ramírez-Lucas, A.; Díaz, J. A.; Sánchez, P.; Romero, A. CO_2 capture in different carbon materials. *Environ. Sci. Technol.* **2012**, *46*, 7407−7414.

(13) Wilson, S. M. W.; Tezel, F. H. Direct Dry Air Capture of CO_2 Using VTSA with Faujasite Zeolites. *Ind. Eng. Chem. Res.* **2020**, *59*, 8783−8794.

(14) Yang, L.; Shi, C.; Li, L.; Li, Y. High-throughput model-building and screening of zeolitic imidazolate frameworks for CO_2 capture from flue gas. *Chin. Chem. Lett.* **2020**, *31*, 227−230.

(15) Liu, J.; Wei, Y.; Zhao, Y. Trace carbon dioxide capture by metal−organic frameworks. *ACS Sustain. Chem. Eng.* **2019**, *7*, 82−93.

(16) Sayari, A.; Belmabkhout, Y.; Serna-Guerrero, R. Flue gas treatment via CO_2 adsorption. *Chem. Eng. J.* **2011**, *171*, 760−774.

(17) Kumar, A.; Madden, D. G.; Lusi, M.; Chen, K.-J.; Daniels, E. A.; Curtin, T.; Perry, J. J.; Zaworotko, M. J. Direct air capture of CO_2 by

physisorbent materials. *Angew. Chem., Int. Ed.* **2015**, *54*, 14372−14377.
(18) Stolaroff, J. K.; Keith, D. W.; Lowry, G. V. Carbon dioxide capture from atmospheric air using sodium hydroxide spray. *Environ. Sci. Technol.* **2008**, *42*, 2728−2735.
(19) Zeman, F. S.; Lackne, K. S. Capturing carbon dioxide directly from the atmosphere. *World Resour. Rev.* **2004**, *16*, 157−172.
(20) Zeman, F. Reducing the cost of Ca-based direct air capture of CO_2. *Environ. Sci. Technol.* **2014**, *48*, 11730−11735.
(21) Luo, C.; Zheng, Y.; Ding, N.; Wu, Q. L.; Zheng, C. G. SGCS-made ultrafine CaO/Al_2O_3 sorbent for cyclic CO_2 capture. *Chin. Chem. Lett.* **2011**, *22*, 615−618.
(22) Veselovskaya, J. V.; Lysikov, A. I.; Netskina, O. V.; Kuleshov, D. V.; Okunev, A. G. K_2CO_3-Containing Composite Sorbents Based on Thermally Modified Alumina: Synthesis, Properties, and Potential Application in a Direct Air Capture/Methanation Process. *Ind. Eng. Chem. Res.* **2020**, *59*, 7130−7139.
(23) Rochelle, G. T. Amine scrubbing for CO_2 capture. *Science* **2009**, *325*, 1652−1654.
(24) Shi, X. Y.; Xiao, H.; Azarabadi, H.; Song, J. Z.; Wu, X. L.; Chen, X.; Lackner, K. S. Sorbents for Direct Capture of CO_2 from Ambient Air. *Angew. Chem., Int. Ed.* **2020**, *59*, 6984−7006.
(25) Anyanwu, J.-T.; Wang, Y.; Yang, R. T. Amine-Grafted Silica Gels for CO_2 Capture Including Direct Air Capture. *Ind. Eng. Chem. Res.* **2020**, *59*, 7072−7079.
(26) Song, T.; Zhao, H.; Hu, Y.; Sun, N.; Zhang, H. Facile assembly of mesoporous silica nanoparticles with hierarchical pore structure for CO_2 capture. *Chin. Chem. Lett.* **2019**, *30*, 2347−2350.
(27) Wang, J.; Huang, H.; Wang, M.; Yao, L.; Qiao, W.; Long, D.; Ling, L. Direct Capture of Low-Concentration CO_2 on Mesoporous Carbon-Supported Solid Amine Adsorbents at Ambient Temperature. *Ind. Eng. Chem. Res.* **2015**, *54*, 5319−5327.
(28) Sanz-Pérez, E. S.; Fernández, A.; Arencibia, A.; Calleja, G.; Sanz, R. Hybrid amine-silica materials: Determination of N content by ^{29}Si NMR and application to direct CO_2 capture from air. *Chem. Eng. J.* **2019**, *373*, 1286−1294.
(29) Drese, J. H.; Choi, S.; Lively, R. P.; Koros, W. J.; Fauth, D. J.; Gray, M. L.; Jones, C. W. Synthesis−structure−property relationships for hyperbranched aminosilica CO_2 adsorbents. *Adv. Funct. Mater.* **2009**, *19*, 3821−3832.
(30) Yang, H.; Singh, M.; Schaefer, J. Humidity-Swing Mechanism for CO_2 Capture from Ambient Air. *Chem. Commun.* **2018**, *54*, 4915−4918.
(31) Song, J.; Liu, J.; Zhao, W.; Chen, Y.; Xiao, H.; Shi, X.; Liu, Y.; Chen, X. Quaternized Chitosan/PVA Aerogels for Reversible CO_2 Capture from Ambient Air. *Ind. Eng. Chem. Res.* **2018**, *57*, 4941−4948.
(32) Zhang, S.; Shen, Y.; Wang, L.; Chen, J.; Lu, Y. Phase change solvents for post-combustion CO_2 capture: Principle, advances, and challenges. *Appl. Energy* **2019**, *239*, 876−897.
(33) Ye, Q.; Wang, X.; Lu, Y. Q. Screening and evaluation of novel biphasic solvents for energy-efficient post-combustion CO_2 capture. *Int. J. Greenhouse Gas Control* **2015**, *39*, 205−214.
(34) Xu, Z.; Wang, S.; Chen, C. CO_2 absorption by biphasic solvents: Mixtures of 1, 4-Butanediamine and 2-(Diethylamino)-ethanol. *Int. J. Greenhouse Gas Control* **2013**, *16*, 107−115.
(35) Pinto, D. D. D.; Zaidy, S. A. H.; Hartono, A.; Svendsen, H. F. Evaluation of a phase change solvent for CO_2 capture: Absorption and desorption tests. *Int. J. Greenhouse Gas Control* **2014**, *28*, 318−327.
(36) Ciftja, A. F.; Hartono, A.; Svendsen, H. F. Experimental study on phase change solvents in CO_2 capture by NMR spectroscopy. *Chem. Eng. Sci.* **2013**, *102*, 378−386.
(37) Ye, J.; Jiang, C.; Chen, H.; Shen, Y.; Zhang, S.; Wang, L.; Chen, J. Novel biphasic solvent with tunable phase separation for CO_2 capture: Role of water content in mechanism, kinetics, and energy penalty. *Environ. Sci. Technol.* **2019**, *53*, 4470−4479.
(38) Rangwala, H. A.; Morrell, B. R.; Mather, A. E.; Otto, M. D. Absorption of CO_2 into aqueous tertiary amine/MEA solutions. *Can. J. Chem. Eng.* **2009**, *70*, 482−490.
(39) Wang, L.; Zhang, Y.; Wang, R.; Li, Q.; Zhang, S.; Li, M.; Liu, J.; Chen, B. Advanced monoethanolamine absorption using sulfolane as a phase splitter for CO_2 capture. *Environ. Sci. Technol.* **2018**, *52*, 14556−14563.
(40) Wang, L.; Liu, S.; Wang, R.; Li, Q.; Zhang, S. Regulating Phase Separation Behavior of a DEEA−TETA Biphasic Solvent Using Sulfolane for Energy-Saving CO_2 Capture. *Environ. Sci. Technol.* **2019**, *53*, 12873−12881.
(41) Liu, F.; Shen, Y.; Shen, L.; Sun, C.; Chen, L.; Wang, Q.; Li, S.; Li, W. Novel Amino Functionalized Ionic Liquid/Organic Solvent with low viscosity for CO_2 capture. *Environ. Sci. Technol.* **2020**, *54*, 3520−3529.
(42) Zhang, X.; Zhang, X.; Dong, H.; Zhao, Z.; Zhang, S.; Huang, Y. Carbon capture with ionic liquids: overview and progress. *Energy Environ. Sci.* **2012**, *5*, 6668−6681.
(43) Hasib-ur-Rahman, M.; Siaj, M.; Larachi, F. CO_2 capture in alkanolamine/room-temperature ionic liquid emulsions: A viable approach with carbamate crystallization and curbed corrosion behavior. *Int. J. Greenhouse Gas Control* **2012**, *6*, 246−252.
(44) Hasib-ur-Rahman, M.; Larachi, F. CO_2 capture in alkanol-amine-RTIL blends via carbamate crystallization: route to efficient regeneration. *Environ. Sci. Technol.* **2012**, *46*, 11443−11450.
(45) Iliuta, I.; Hasib-ur-Rahman, M.; Larachi, F. CO_2 absorption in diethanolamine/ionic liquid emulsions−chemical kinetics and mass transfer study. *Chem. Eng. J.* **2014**, *240*, 16−23.
(46) Kim, Y. E.; Park, J. H.; Yun, S. H.; Nam, S. C.; Jeong, S. K.; Yoon, Y. I. Carbon dioxide absorption using a phase transitional alkanolamine−alcohol mixture. *J. Ind. Eng. Chem.* **2014**, *20*, 1486−1492.
(47) Barzagli, F.; Mani, F.; Peruzzini, M. Efficient CO_2 absorption and low temperature desorption with non-aqueous solvents based on 2-amino-2-methyl-1-propanol (AMP). *Int. J. Greenhouse Gas Control* **2013**, *16*, 217−223.
(48) Barzagli, F.; Lai, S.; Mani, F. CO_2 capture by liquid solvents and their regeneration by thermal decomposition of the solid carbonated derivatives. *Chem. Eng. Technol.* **2013**, *36*, 1847−1852.
(49) Zheng, S.; Tao, M.; Liu, Q.; Ning, L.; He, Y.; Shi, Y. Capturing CO_2 into the precipitate of a phase-changing solvent after absorption. *Environ. Sci. Technol.* **2014**, *48*, 8905−8910.
(50) Malhotra, D.; Koech, P. K.; Heldebrant, D. J.; Cantu, D. C.; Zheng, F.; Glezakou, V.-A.; Rousseau, R. Reinventing Design Principles for Developing Low-Viscosity Carbon Dioxide-Binding Organic Liquids for Flue Gas Clean Up. *ChemSusChem* **2017**, *10*, 636−642.
(51) Tan, Y. H.. Study of CO_2-absorption into thermomorphic lipophilic amine solvents [D]. Master's Thesis, Technische Universität Dortmund, Dortmund, Germany, 2010. DOI: 10.17877/DE290R-8236 (accessed 2020-07-23).
(52) Zhang, J. F. Study on CO_2 capture using thermomorphic biphasic solvents with energy efficient regeneration [D]. Master's Thesis, Technische Universität Dortmund, Dortmund, Germany, 2014. DOI: 10.17877/DE290R-7004 (accessed 2020-07-23).
(53) Gadikota, G. Multiphase carbon mineralization for the reactive separation of CO_2 and directed synthesis of H_2. *Nat. Rev. Chem.* **2020**, *4*, 78−89.
(54) Custelcean, R.; Williams, N. J.; Seipp, C. A. Aqueous Sulfate Separation by Crystallization of Sulfate−Water Clusters. *Angew. Chem., Int. Ed.* **2015**, *54*, 10525−9.
(55) Xiao, C.; Khayambashi, A.; Wang, S. Separation and Remediation of $^{99}TcO_4^-$ from Aqueous Solutions. Chem. *Mater* **2019**, *31*, 3863−3877.
(56) Chen, X. J.; Dai, X.; Xie, R. Z.; Li, J.; Khayambashi, A.; Xu, L.; Yang, C.; Shen, N. N.; Wang, Y. X.; He, L. W.; Zhang, Y. G.; Xiao, C. L.; Chai, Z. F.; Wang, S. A. Chromate separation by selective crystallization. *Chin. Chem. Lett.* **2020**, *31*, 1974−1977.
(57) Thiele, J.; Dralle, E. Zur Kenntniss des Amidoguanidins. I. Condensationsproducte des Amidoguanidins mit Aldehyden und Ketonen der Fettreihe. *Justus Liebigs Ann. Chem.* **1898**, *302*, 275−299.

https://dx.doi.org/10.1021/acsomega.0c02460
ACS Omega 2020, 5, 20428−20437

(58) Brethomé, F. M.; Williams, N. J.; Seipp, C. A.; Kidder, M. K.; Custelcean, R. Direct air capture of CO_2 via aqueous-phase absorption and crystalline-phase release using concentrated solar power. *Nat. Energy* **2018**, *3*, 553−559.
(59) Williams, N. J.; Seipp, C. A.; Brethomé, F. M.; Ma, Y.-Z.; Ivanov, A. S.; Bryantsev, V. S.; Kidder, M. K.; Martin, H. J.; Holguin, E.; Garrabrant, K. A.; Custelcean, R. CO_2 capture via crystalline hydrogen-bonded bicarbonate dimers. *Chem* **2019**, *5*, 719−730.
(60) Garrabrant, K. A.; Williams, N. J.; Holguin, E.; Brethomé, F. M.; Tsouris, C.; Custelcean, R. Energy-Efficient CO_2 Capture from Flue Gas by Absorption with Amino Acids and Crystallization with a Bis-Iminoguanidine. *Ind. Eng. Chem. Res.* **2019**, *58*, 10510−10515.
(61) Jiang, J.; Zhao, B.; Zhuo, Y.; Wang, S. Experimental study of CO_2 absorption in aqueous MEA and MDEA solutions enhanced by nanoparticles. *Int. J. Greenhouse Gas Control* **2014**, *29*, 135−141.
(62) Carroll, J. J.; Slupsky, J. D.; Mather, A. E. The solubility of carbon dioxide in water at low pressure. *J. Phys. Chem. Ref. Data* **1991**, *20*, 1201−1209.
(63) Wang, X.; Conway, W.; Burns, R.; McCann, N.; Maeder, M. Comprehensive study of the hydration and dehydration reactions of carbon dioxide in aqueous solution. *J. Phys. Chem. A* **2010**, *114*, 1734−1740.
(64) McCann, N.; Maeder, M.; Hasse, H. A calorimetric study of carbamate formation. *J. Chem. Thermodyn.* **2011**, *43*, 664−669.
(65) Hale, J. D.; Izatt, R. M.; Christensen, J. J. Calorimetric study of the heat of ionization of water at 25°. *J. Phys. Chem.* **1963**, *67*, 2605−2608.
(66) Rodriguez-Navarro, C.; Ruiz-Agudo, E.; Luque, A.; Rodriguez-Navarro, A. B. Ortega-Huertas M. Thermal decomposition of calcite: Mechanisms of formation and textural evolution of CaO nanocrystals. *Am. Miner.* **2009**, *94*, 578−593.

https://dx.doi.org/10.1021/acsomega.0c02460
ACS Omega 2020, 5, 20428−20437